Uncertainty Propagation in the N-body Problem using Dromo Elements

Javier Hernando-Ayuso[a,*], Claudio Bombardelli[b], Giulio Baù[c]

[a] *The University of Tokyo, 7-3-1 Hongo, Bunkyo-ku, Tokyo 113-8656, Japan.*
[b] *Technical University of Madrid, Plaza Cardenal Cisneros, 3, Madrid 28040, Spain*
[c] *Department of Mathematics, University of Pisa, Largo Pontecorvo 5, Pisa I-56127, Italy*

Abstract

Reliable and efficient uncertainty propagation is crucial for the task of monitoring possible impacts of Near Earth Asteroids with our planet. It is well known that a switch of the primary body can greatly reduce the numerical truncation error in the case of planetary flybys. In the present work, the advantages of performing a primary body switch in the uncertainty propagation problem are explored. For this purpose, first we present the linear uncertainty propagation using Dromo formulation, which has been shown in previous works to have a satisfactory performance when propagating the orbit uncertainty of Near Earth Asteroids. Next, we introduce the concept of primary body switch for the uncertainty propagation problem. The algorithm is based on the following procedure. We sample the initial orbit uncertainty distribution and linearly propagate the samples, considering the N-body gravitational influence. A primary body switch, which is a nonlinear mapping, is performed for all the samples at a threshold distance from the approaching planet, the Earth. The orbit of the samples is then linearly propagated with respect to the Earth using the Dromo formulation until the threshold distance is reached again. Finally, the propagation center is changed back to the heliocentric frame and the linear propagation continues. We apply the proposed method to an extensive set of

*Corresponding author
Email addresses: javier.hernando@ac.jaxa.jp (Javier Hernando-Ayuso), claudio.bombardelli@upm.es (Claudio Bombardelli), giulio.bau@unipi.it (Giulio Baù)

asteroids that approach the Earth. Results suggest that the average error of the linear propagation can be reduced up to a factor of 30 when compared to a purely heliocentric linear propagation using Dromo elements.
Keywords: Covariance Propagation, Dromo, State Transition Matrix, Near Earth Asteroids, Primary body switch

1. Introduction

Orbit uncertainty propagation is a key aspect of Astrodynamics that has been receiving increasing attention in the last years. For some applications, it is not enough to just analyze the nominal orbit of an object, and it becomes paramount to carefully consider the deviation from the real and the predicted orbit. In particular, in the context of planetary defense, reliable and efficient uncertainty propagation is crucial for the task of monitoring possible impacts of Near Earth Asteroids (NEAs) with our planet.

When the uncertainty is small, the probability distribution function (pdf) is usually modeled as Gaussian because of the central limit theorem and because its analytical properties, mainly preservation of Gaussianity under linear transformations. Unfortunately, the orbital motion is strongly nonlinear and the assumption of a Gaussian distribution propagated linearly eventually loses validity. When this happens, in general one must obtain the pdf by solving complicated partial differential equations, like the Fokker-Plank Equation [1, pp. 192-202], or use another method to accurately calculate the evolution of the orbit pdf. For instance, Park et al. [2] proposed generalizing the state transition matrix (STM) to higher orders by constructing state transition tensors. The use of Differential Algebra (DA) has also been proposed [3] and applied to real cases like the 2029 close approach of the asteroid Apophis. Another possibility is to model the orbit uncertainty as a sum of Gaussian kernels in the Gaussian Mixture Model (GMM) [4].

There is a whole family of non-intrusive methods that exploit already existing orbit propagation tools. The most elementary method one could think of is

a simple Monte Carlo (MC) method, which propagates random samples of the initial distribution. If the samples are not random but correspond to carefully chosen points, computational time can be greatly reduced by the use of the Unscented Kalman Filter [5]. The solution can be conveniently projected in an orthonormal basis using Polynomial Chaos Expansions (PCE), and the components in the new basis can be calculated from propagation of a reduced number of samples [6]. Vittaldev and Russell proposed a combination of GMM and PCE [7]. Kriging, a method for interpolation from discrete data, has also been applied for orbit uncertainty propagation [8]. When studying the orbit uncertainty of NEAs, Milani et al introduced the concept of Line Of Variations (LOV), a one-dimensional sampling along a carefully chosen direction that accounts for most of the orbit uncertainty [9].

Some techniques are possible to extend the validity of linear methods, which are usually faster than the methods mentioned above. Junkins et al. [10] pointed out that the accuracy of the predicted covariance depends on the set of variables that constitute the state vector. They proposed the use of equinoctial elements substituting the classical Cartesian representation, but curvilinear coordinates have also been proven to ameliorate the problem (see [11, 12, 13, 14, 15] for instance).

One relatively recent orbital motion formulation that may be very promising for uncertainty propagation is Dromo, proposed by Peláez et al. in 2007 [16] and considerably improved in subsequent works by Urrutxua et al. [17], Baù et al. in 2013 [18], 2014 [19], and 2015 [20]. It employs seven non-singular orbital elements and a fictitious time derived from a second order Sundman transformation. It has been shown that Dromo exhibits an excellent performance in terms of numerical propagation of orbits. Using this formulation, the *linear* propagation of the uncertainty of NEAs subject to N-body perturbation was presented recently and shown to drastically improve its Cartesian counterpart [21]. The method has been applied to Earth-bounded orbits as well, obtaining satisfactory results [22].

While linearization with the original Dromo formulation is possible [23],

it leads to problems of time synchrony in the propagated pdf [24]. The first step in order to make the formulation applicable to covariance propagation in time was to choose time as the independent variable. This is crucial when the covariance propagation process involves time-dependent perturbations whose time-derivative needs to be evaluated. The propagation of asteroid orbits, for instance, requires the computation of N-bodies gravitational perturbations obtained from time-dependent ephemerides. Next, one has to construct a state transition matrix (STM) in Dromo elements and obtain the fundamental (linear) differential equation that governs its time evolution by computing the partial derivatives of the perturbing accelerations with respect to the Dromo state variables. Once the time evolution of the state transition matrix is obtained, the covariance matrix propagation can be carried out analytically, effectively propagating the initial orbit uncertainty into the future. The details of this approach can be found in [21] and [22].

It is well known that a primary body switch can greatly reduce the numerical truncation error in the cases of planets flybys. Recently, Amato et al. [25] showed that the distance at which the primary body switch is performed when using a Dromo formulation strongly affects the accuracy of the calculations. The existence of a non-trivial optimum switch distance was also reported. This distance does not coincide with the size of the Sphere of Influence of the approached planet, but is actually greater.

In the present work, the advantages of a primary body switch on the propagation of orbit uncertainty are explored, under the assumption of a deterministic dynamical system. When propagating the uncertainty of the orbital motion, a primary body switch seeks reducing the third-body gravity linearization error pointed out by Hernando-Ayuso and Bombardelli [21]. To highlight the benefit of the switch, we employ a Monte Carlo method with random sampling of the initial pdf. Each sample is propagated linearly around the mean orbit, and the nonlinear function that describes the primary body switch in Dromo elements allows reducing the uncertainty propagation error. Without loss of generality, this strategy can be combined with other methods introduced above (LOV,

GMM, STT, PCE, DA, etc) reducing the number of terms or samples needed for a given accuracy, or decreasing the error for an equivalent computational time.

We present the Dromo formulation and the linear propagation around a reference orbit in sections 2 and 3, respectively. We then introduce in section 4 the concept of primary body switch for the uncertainty propagation problem. Finally, in sections 5 and 6, we present and discuss the results of the primary body switch when propagating the uncertainty of a group of selected asteroids.

2. Dromo formulation

Let us consider a particle of negligible mass orbiting around a primary of gravitational parameter μ. Let us employ, from now on and unless specified, $\tilde{r} = 1$ au as unit of distance, and $1/\tilde{n}$ as unit of time (τ), where $\tilde{n}$ is the angular rate of a *circular* orbit with radius equal to the reference radius $\tilde{r}$:

$$\tilde{n} = \sqrt{\frac{\mu}{\tilde{r}^3}}. \tag{1}$$

In this canonical system of units, the gravitational parameter of the primary becomes unity.

2.1. Fictitious time

The Dromo formulation is characterized by the use of a fictitious time σ as independent variable as given by the second-order Sundman transformation:

$$\frac{\mathrm{d}\tau}{\mathrm{d}\sigma} = \frac{r^2}{h} \tag{2}$$

where h is the angular momentum and r corresponds to the orbital radius. The fictitious time σ is related to the osculating true anomaly ν by

$$\sigma = \nu + \beta. \tag{3}$$

That is, the fictitious time evolves as the osculating true anomaly plus a drift β caused by orbital perturbations. Without any loss of generality, we can set

the value of β for the initial epoch equal to zero. Note that for the uncertainty propagation problem we justified in [21] the convenience of using the real time τ as independent variable. Therefore, we will consider σ as a variable that depends on time, and propagate it together with the rest of the Dromo elements.

2.2. Dromo elements

To avoid singularities in the description of the orbital motion, seven generalized orbital elements are used in this formulation.

The first three Dromo elements are defined as:

$$q_1 = \frac{e}{h}\cos\beta, \tag{4}$$

$$q_2 = \frac{e}{h}\sin\beta, \tag{5}$$

$$q_3 = \frac{1}{h}, \tag{6}$$

where e corresponds to the magnitude of the eccentricity vector $\boldsymbol{e}$.

The four remaining generalized orbital elements are the Euler-Rodrigues parameters characterizing the rotation associated to the matrix $\boldsymbol{P}$. This rotation brings an *intermediate frame* $\mathcal{P}$ (having two axes constantly lying in the instantaneous orbital plane of the particle) to overlap with a reference inertial frame ($\mathcal{I}$). In the classical Dromo formulation [16], the intermediate frame was chosen to coincide with the local-vertical local-horizontal (LVLH) orbital frame $\mathcal{R}$ at $\tau = 0$. Here we choose $\mathcal{P}$ in such a way that it coincides with the perifocal frame at $\tau = 0$, as done in Ref. [17]. The matrix $\boldsymbol{P}$ reads

$$\boldsymbol{P} = \begin{bmatrix} 1-2\left(q_5^2+q_6^2\right) & 2\left(q_4q_5-q_6q_7\right) & 2\left(q_4q_6+q_5q_7\right) \\ 2\left(q_4q_5+q_6q_7\right) & 1-2\left(q_4^2+q_6^2\right) & 2\left(q_5q_6-q_4q_7\right) \\ 2\left(q_4q_6-q_5q_7\right) & 2\left(q_5q_6+q_4q_7\right) & 1-2\left(q_4^2+q_5^2\right) \end{bmatrix}. \tag{7}$$

An additional rotation matrix $\boldsymbol{Q}$ brings the orbital frame $\mathcal{R}$ to overlap with the intermediate frame $\mathcal{P}$ through a rotation of $-\sigma$ around the common z-axis, which is oriented towards the angular momentum vector:

$$\boldsymbol{Q} = \begin{bmatrix} \cos\sigma & -\sin\sigma & 0 \\ \sin\sigma & \cos\sigma & 0 \\ 0 & 0 & 1 \end{bmatrix}. \tag{8}$$

Finally, the rotation from the $\mathcal{I}$ to the $\mathcal{R}$ frame can be built as the composition of the rotations previously introduced, and is characterized by the matrix $\boldsymbol{R}$ given by

$$\boldsymbol{R} = \boldsymbol{P}\,\boldsymbol{Q}. \tag{9}$$

The Euler-Rodrigues parameters can be related to the classical orbital elements (i inclination, Ω right ascension of the ascending node, and ω argument of periapsis) as follows:

$$q_4 = \sin\frac{i}{2}\cos\frac{\Omega-\omega+\beta}{2}, \tag{10}$$

$$q_5 = \sin\frac{i}{2}\sin\frac{\Omega-\omega+\beta}{2}, \tag{11}$$

$$q_6 = \cos\frac{i}{2}\sin\frac{\Omega+\omega-\beta}{2}, \tag{12}$$

$$q_7 = \cos\frac{i}{2}\cos\frac{\Omega+\omega-\beta}{2}, \tag{13}$$

where β was introduced in Eq. (3).

The inertial reference frame $\mathcal{I}$, the intermediate frame $\mathcal{P}$ and the LVLH frame $\mathcal{R}$, as well as the rotations that relate them, are shown in figures 1 and 2.

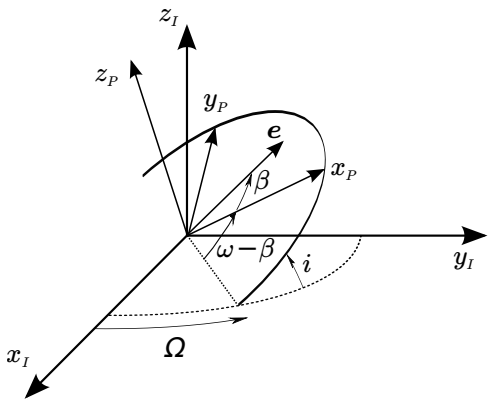

Figure 1: Inertial ($\mathcal{I} = \langle x_{\mathcal{I}}, y_{\mathcal{I}}, z_{\mathcal{I}}\rangle$) and intermediate ($\mathcal{P} = \langle x_{\mathcal{P}}, y_{\mathcal{P}}, z_{\mathcal{P}}\rangle$) frames.

An alternative derivation of Dromo elements from the inertial Cartesian state is provided in Appendix A.

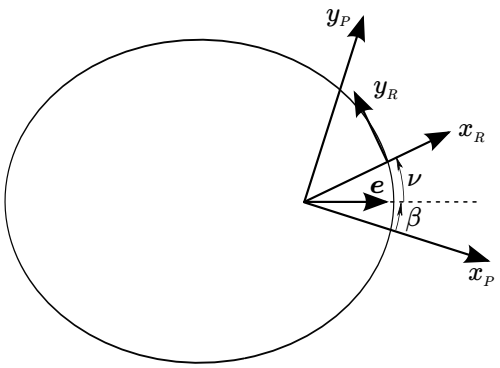

Figure 2: Intermediate ($\mathcal{P} = \langle x_\mathcal{P}, y_\mathcal{P}, z_\mathcal{P} \rangle$) and LVLH ($\mathcal{R} = \langle x_\mathcal{R}, y_\mathcal{R}, z_\mathcal{R} \rangle$) frames. Note that $z_\mathcal{R} \equiv z_\mathcal{P}$.

2.3. Equations of Motion

After introducing the Dromo state vector $\boldsymbol{q} = (q_1, \ldots, q_7, \sigma)^\top$, the equations of motion in the presence of a perturbing acceleration $\boldsymbol{f}(\boldsymbol{q}, \tau) = (f_r, f_\theta, f_h)^\top$ expressed in the $\mathcal{R}$ frame can be written as (see [22])

$$\frac{\mathrm{d}\boldsymbol{q}}{\mathrm{d}\tau} = \boldsymbol{g}(\boldsymbol{q}, \boldsymbol{f}(\boldsymbol{q}, \tau)) \tag{14}$$

where

$$g_1 = \frac{\mathrm{d}q_1}{\mathrm{d}\tau} = \frac{f_\theta}{s}(s + q_3)\cos\sigma + f_r \sin\sigma, \tag{15a}$$

$$g_2 = \frac{\mathrm{d}q_2}{\mathrm{d}\tau} = \frac{f_\theta}{s}(s + q_3)\sin\sigma - f_r \cos\sigma, \tag{15b}$$

$$g_3 = \frac{\mathrm{d}q_3}{\mathrm{d}\tau} = -f_\theta \frac{q_3}{s}, \tag{15c}$$

$$g_4 = \frac{\mathrm{d}q_4}{\mathrm{d}\tau} = \frac{f_h}{2s}(q_7 \cos\sigma - q_6 \sin\sigma), \tag{15d}$$

$$g_5 = \frac{\mathrm{d}q_5}{\mathrm{d}\tau} = \frac{f_h}{2s}(q_6 \cos\sigma + q_7 \sin\sigma), \tag{15e}$$

$$g_6 = \frac{\mathrm{d}q_6}{\mathrm{d}\tau} = -\frac{f_h}{2s}(q_5 \cos\sigma - q_4 \sin\sigma), \tag{15f}$$

$$g_7 = \frac{\mathrm{d}q_7}{\mathrm{d}\tau} = -\frac{f_h}{2s}(q_4 \cos\sigma + q_5 \sin\sigma), \tag{15g}$$

$$g_8 = \frac{\mathrm{d}\sigma}{\mathrm{d}\tau} = q_3 s^2. \tag{15h}$$

2.4. Dromo elements inverse transformations

After obtaining the time evolution of the Dromo elements, it is convenient to obtain a more intuitive representation of the state. To this end, we employ the inverse of the transformation described by Eqs. (4–6) and Eqs. (10–13) to express the classical orbital elements as a function of the Dromo elements:

$$a = \frac{1}{q_3^2 - q_1^2 - q_2^2}, \tag{16}$$

$$e = \frac{1}{q_3}\sqrt{q_1^2 + q_2^2}, \tag{17}$$

$$i = \cos^{-1}\left(1 - 2\left(q_4^2 + q_5^2\right)\right), \tag{18}$$

$$\Omega = \operatorname{atan2}\left(q_5, q_4\right) + \operatorname{atan2}\left(q_6, q_7\right), \tag{19}$$

$$\omega = \operatorname{atan2}\left(q_2, q_1\right) + \operatorname{atan2}\left(q_6, q_7\right) - \operatorname{atan2}\left(q_5, q_4\right), \tag{20}$$

$$\nu = \sigma - \operatorname{atan2}\left(q_2, q_1\right). \tag{21}$$

It is also possible to express the inertial Cartesian position $\boldsymbol{r} = (x, y, z)^\top$ and velocity $\boldsymbol{v} = (v_x, v_y, v_z)^\top$ as a function of the Dromo elements. This relation can be written in compact form as

$$\boldsymbol{r} = \boldsymbol{R}\begin{pmatrix} r \\ 0 \\ 0 \end{pmatrix} = r\,\boldsymbol{P}\begin{pmatrix} \cos\sigma \\ \sin\sigma \\ 0 \end{pmatrix}, \tag{22}$$

$$\boldsymbol{v} = \boldsymbol{R}\begin{pmatrix} u \\ s \\ 0 \end{pmatrix} = \boldsymbol{P}\begin{pmatrix} -q_2 - q_3\sin\sigma \\ q_1 + q_3\cos\sigma \\ 0 \end{pmatrix}, \tag{23}$$

where the orbital radius r takes the expression

$$r = \frac{1}{q_3 s}. \tag{24}$$

Finally, s and u represent the transversal and radial components of the particle velocity, respectively, and obey

$$s = q_3 + q_1\cos\sigma + q_2\sin\sigma, \tag{25}$$

$$u = -\frac{\partial s}{\partial \sigma} = q_1\sin\sigma - q_2\cos\sigma. \tag{26}$$

3. Linear propagation with Dromo

An orbit $\boldsymbol{q}$ close to a reference orbit $\boldsymbol{q}_{\rm ref}$ can be linearly propagated via the State Transition Matrix (STM) as

$$\boldsymbol{q}\left(\tau\right) = \boldsymbol{q}_{\rm ref}\left(\tau\right) + \boldsymbol{\Phi}\left(\tau,\tau_0\right)\left(\boldsymbol{q}\left(\tau_0\right) - \boldsymbol{q}_{\rm ref}\left(\tau_0\right)\right). \tag{27}$$

The evolution of the STM is given by

$$\frac{\mathrm{d}\boldsymbol{\Phi}(\tau,\tau_0)}{\mathrm{d}\tau} = \boldsymbol{G}\left(\boldsymbol{q}_{\rm ref}\left(\tau\right),\tau\right)\boldsymbol{\Phi}(\tau,\tau_0), \quad \boldsymbol{\Phi}(\tau_0,\tau_0) = \boldsymbol{I}_8 \tag{28}$$

which must be integrated together with Eq. (14), and where $\boldsymbol{I}_8$ is the eight-dimensional identity matrix. The gradient matrix $\boldsymbol{G}$ corresponds to the following total derivative evaluated on the reference orbit

$$\boldsymbol{G} = \frac{\mathrm{d}\boldsymbol{g}}{\mathrm{d}\boldsymbol{q}} = \frac{\partial \boldsymbol{g}}{\partial \boldsymbol{q}} + \frac{\partial \boldsymbol{g}}{\partial \boldsymbol{f}}\frac{\partial \boldsymbol{f}}{\partial \boldsymbol{q}} \tag{29}$$

where $\boldsymbol{f}$ must be expressed in the $\mathcal{R}$ reference system.

The derivative $\frac{\partial \boldsymbol{g}}{\partial \boldsymbol{q}}$ must be calculated for constant $\boldsymbol{f}$:

$$\frac{\partial \boldsymbol{g}}{\partial \boldsymbol{q}} = \begin{bmatrix}
-\frac{f_\theta q_3 \cos^2\sigma}{s^2} & -\frac{f_\theta q_3 \cos\sigma\sin\sigma}{s^2} & f_\theta\frac{s-q_3}{s^2}\cos\sigma & 0 & 0 & 0 & 0 & \frac{\partial g_1}{\partial\sigma} \\
-\frac{f_\theta q_3 \cos\sigma\sin\sigma}{s^2} & -\frac{f_\theta q_3 \sin^2\sigma}{s^2} & f_\theta\frac{s-q_3}{s^2}\sin\sigma & 0 & 0 & 0 & 0 & \frac{\partial g_2}{\partial\sigma} \\
\frac{f_\theta q_3 \cos\sigma}{s^2} & \frac{f_\theta q_3 \sin\sigma}{s^2} & -f_\theta\frac{s-q_3}{s^2} & 0 & 0 & 0 & 0 & -f_\theta\frac{u}{s}\frac{q_3}{s} \\
-\frac{g_4\cos\sigma}{s} & -\frac{g_4\sin\sigma}{s} & -\frac{g_4}{s} & 0 & 0 & -\frac{f_h\sin\sigma}{2s} & \frac{f_h\cos\sigma}{2s} & \frac{g_4 u - g_5 s}{s} \\
-\frac{g_5\cos\sigma}{s} & -\frac{g_5\sin\sigma}{s} & -\frac{g_5}{s} & 0 & 0 & \frac{f_h\cos\sigma}{2s} & \frac{f_h\sin\sigma}{2s} & \frac{g_5 u + g_4 s}{s} \\
-\frac{g_6\cos\sigma}{s} & -\frac{g_6\sin\sigma}{s} & -\frac{g_6}{s} & \frac{f_h\sin\sigma}{2s} & -\frac{f_h\cos\sigma}{2s} & 0 & 0 & \frac{g_6 u - g_7 s}{s} \\
-\frac{g_7\cos\sigma}{s} & -\frac{g_7\sin\sigma}{s} & -\frac{g_7}{s} & -\frac{f_h\cos\sigma}{2s} & -\frac{f_h\sin\sigma}{2s} & 0 & 0 & \frac{g_7 u + g_6 s}{s} \\
2q_3 s\cos\sigma & 2q_3 s\sin\sigma & s^2 + 2q_3 s & 0 & 0 & 0 & 0 & -2q_3 s\, u
\end{bmatrix}, \tag{30}$$

with

$$\frac{\partial g_1}{\partial\sigma} = f_r\cos\sigma + f_\theta\left(\frac{u}{s}\frac{q_3}{s}\cos\sigma - \left(1+\frac{q_3}{s}\right)\sin\sigma\right), \tag{31}$$

$$\frac{\partial g_2}{\partial\sigma} = f_r\sin\sigma + f_\theta\left(\frac{u}{s}\frac{q_3}{s}\sin\sigma + \left(1+\frac{q_3}{s}\right)\cos\sigma\right). \tag{32}$$

The second derivative, $\frac{\partial \boldsymbol{g}}{\partial \boldsymbol{f}}$, is calculated considering a constant Dromo state vector:

$$\frac{\partial \boldsymbol{g}}{\partial \boldsymbol{f}} = \begin{bmatrix} \sin\sigma & \left(1+\frac{q_3}{s}\right)\cos\sigma & 0 \\ -\cos\sigma & \left(1+\frac{q_3}{s}\right)\sin\sigma & 0 \\ 0 & -\frac{q_3}{s} & 0 \\ 0 & 0 & \frac{1}{2s}\left(q_7\cos\sigma - q_6\sin\sigma\right) \\ 0 & 0 & \frac{1}{2s}\left(q_6\cos\sigma + q_7\sin\sigma\right) \\ 0 & 0 & -\frac{1}{2s}\left(q_5\cos\sigma - q_4\sin\sigma\right) \\ 0 & 0 & -\frac{1}{2s}\left(q_4\cos\sigma + q_5\sin\sigma\right) \\ 0 & 0 & 0 \end{bmatrix}. \tag{33}$$

Finally, the last derivative $\frac{\partial \boldsymbol{f}}{\partial \boldsymbol{q}}$ depends on the nature of the perturbing accelerations and must be calculated for each of them. Explicit expressions for third-body perturbing accelerations are given in section 3.1.

3.1. N-body perturbation

The N-body perturbing acceleration can be written as

$$\boldsymbol{f} = -\sum_{j=2}^{N-1} \mu_j \frac{\boldsymbol{r}-\boldsymbol{r}_j}{\|\boldsymbol{r}-\boldsymbol{r}_j\|^3} - \sum_{j=2}^{N-1} \mu_j \frac{\boldsymbol{r}_j}{\|\boldsymbol{r}_j\|^3} \tag{34}$$

where $j = 1$ is the primary body already considered in the Dromo formulation and $j = N$ is the propagated object, whose mass is considered negligible with respect to the perturbing bodies. The quantities $\boldsymbol{r}_j$ and μ_j are the position vector and the gravitational parameter of the j^{th} body respectively.

It is important to underline that in order to derive analytical expressions for the 3×8 Jacobian matrix $\frac{\partial \boldsymbol{f}}{\partial \boldsymbol{q}}$, the perturbing acceleration $\boldsymbol{f}$ has to be projected onto the $\mathcal{R}$ reference frame. The representation of the particle position vector with respect to such frame is straightforward:

$$\boldsymbol{r}^{\mathcal{R}} = \left(\frac{1}{q_3 s}, 0, 0\right)^{\top}. \tag{35}$$

The position of the j^{th} body only depends on time and can be obtained using JPL's DE ephemeris [26] or VSOP [27] (*Variations Séculaires des Orbites*

Planétaires), for example. This position is usually expressed as a vector $\boldsymbol{r}_j^{\mathcal{I}}$ with respect to the inertial frame and can be projected onto $\mathcal{R}$ as follows

$$\boldsymbol{r}_j^{\mathcal{R}} = \boldsymbol{R}^\top \boldsymbol{r}_j^{\mathcal{I}}. \tag{36}$$

The derivative of the force components in $\mathcal{R}$ can be obtained by applying the chain rule, if we consider that $\boldsymbol{f}$ depends on $\boldsymbol{q}$ through $\boldsymbol{r}$ and $\boldsymbol{r}_j$:

$$\frac{\partial \boldsymbol{f}}{\partial \boldsymbol{q}} = \frac{\partial \boldsymbol{f}}{\partial \boldsymbol{r}^{\mathcal{R}}} \frac{\partial \boldsymbol{r}^{\mathcal{R}}}{\partial \boldsymbol{q}} + \sum_{j=2}^{N-1} \frac{\partial \boldsymbol{f}}{\partial \boldsymbol{r}_j^{\mathcal{R}}} \frac{\partial \boldsymbol{r}_j^{\mathcal{R}}}{\partial \boldsymbol{q}} \tag{37}$$

Reordering the terms in the summation, we obtain

$$\begin{aligned} \frac{\partial \boldsymbol{f}}{\partial \boldsymbol{q}} = -\sum_{j=2}^{N-1} \mu_j \Bigg\{ & \left(\frac{\boldsymbol{I}_3}{\left\| \boldsymbol{r}^{\mathcal{R}} - \boldsymbol{r}_j^{\mathcal{R}} \right\|^3} - 3 \frac{\left(\boldsymbol{r}^{\mathcal{R}} - \boldsymbol{r}_j^{\mathcal{R}} \right) \left(\boldsymbol{r}^{\mathcal{R}} - \boldsymbol{r}_j^{\mathcal{R}} \right)^\top}{\left\| \boldsymbol{r}^{\mathcal{R}} - \boldsymbol{r}_j^{\mathcal{R}} \right\|^5} \right) \left(\frac{\partial \boldsymbol{r}^{\mathcal{R}}}{\partial \boldsymbol{q}} - \frac{\partial \boldsymbol{r}_j^{\mathcal{R}}}{\partial \boldsymbol{q}} \right) \\ & + \left(\frac{\boldsymbol{I}_3}{\left\| \boldsymbol{r}_j^{\mathcal{R}} \right\|^3} - 3 \frac{\boldsymbol{r}_j^{\mathcal{R}} \boldsymbol{r}_j^{\mathcal{R}\top}}{\left\| \boldsymbol{r}_j^{\mathcal{R}} \right\|^5} \right) \frac{\partial \boldsymbol{r}_j^{\mathcal{R}}}{\partial \boldsymbol{q}} \Bigg\} \end{aligned} \tag{38}$$

where $\boldsymbol{I}_3$ is the 3-dimensional identity matrix, $\boldsymbol{y}\,\boldsymbol{y}^\top$ represents the outer product of the vector $\boldsymbol{y} \in \mathbb{R}^3$ with itself, which results in a 3-dimensional matrix, and

$$\frac{\partial \boldsymbol{r}^{\mathcal{R}}}{\partial \boldsymbol{q}} = \begin{bmatrix} -\frac{\cos\sigma}{q_3 s^2} & -\frac{\sin\sigma}{q_3 s^2} & -\frac{s+q_3}{q_3^2 s^2} & 0 & 0 & 0 & 0 & \frac{u}{q_3 s^2} \\ 0 & 0 & 0 & 0 & 0 & 0 & 0 & 0 \\ 0 & 0 & 0 & 0 & 0 & 0 & 0 & 0 \end{bmatrix}, \tag{39}$$

$$\frac{\partial \boldsymbol{r}_j^{\mathcal{R}}}{\partial \boldsymbol{q}} = \begin{bmatrix} 0 & 0 & 0 & | & \dots & | & | \\ 0 & 0 & 0 & \boldsymbol{Q}^\top \frac{\partial \boldsymbol{P}^\top}{\partial q_4} \boldsymbol{R} \boldsymbol{r}_j^{\mathcal{R}} & \dots & \boldsymbol{Q}^\top \frac{\partial \boldsymbol{P}^\top}{\partial q_7} \boldsymbol{R} \boldsymbol{r}_j^{\mathcal{R}} & \frac{\partial \boldsymbol{Q}^\top}{\partial \sigma} \boldsymbol{Q} \boldsymbol{r}_j^{\mathcal{R}} \\ 0 & 0 & 0 & | & \dots & | & | \end{bmatrix}, \tag{40}$$

with

$$\frac{\partial \boldsymbol{P}}{\partial q_4} = \begin{bmatrix} 0 & 2q_5 & 2q_6 \\ 2q_5 & -4q_4 & -2q_7 \\ 2q_6 & 2q_7 & -4q_4 \end{bmatrix},$$
$$\frac{\partial \boldsymbol{P}}{\partial q_5} = \begin{bmatrix} -4q_5 & 2q_4 & 2q_7 \\ 2q_4 & 0 & 2q_5 \\ -2q_7 & 2q_6 & -4q_5 \end{bmatrix},$$
$$\frac{\partial \boldsymbol{P}}{\partial q_6} = \begin{bmatrix} -4q_6 & -2q_7 & 2q_4 \\ 2q_7 & -4q_6 & 2q_5 \\ 2q_4 & 2q_5 & 0 \end{bmatrix}, \tag{41}$$
$$\frac{\partial \boldsymbol{P}}{\partial q_7} = \begin{bmatrix} 0 & -2q_6 & 2q_5 \\ 2q_6 & 0 & -2q_4 \\ -2q_5 & 2q_4 & 0 \end{bmatrix}.$$

Finally,

$$\frac{\partial \boldsymbol{Q}^\top}{\partial \sigma} = \begin{bmatrix} -\sin\sigma & -\cos\sigma & 0 \\ \cos\sigma & -\sin\sigma & 0 \\ 0 & 0 & 0 \end{bmatrix}. \tag{42}$$

4. Primary body switch

To overcome the limitations of a purely heliocentric linear propagation in the presence of close approaches with planets, we introduce a primary body switch at a threshold distance from the encountering planet. Without loss of generality, we assume that the encountering planet is the Earth.

When employing the primary body switch strategy, the linear propagation is substituted with a hybrid Monte Carlo (MC) method. At the initial epoch, we sample $M = 1000$ random points from the Gaussian distribution described by the nominal orbit and the covariance matrix. For each asteroid, the nominal orbit and covariance matrix are obtained from the NEODyS database, maintained by the University of Pisa and the SpaceDyS company. NEODyS offers this information for two different epochs: *Near middle of observational arc* and

Near present day. We chose the former, aiming to minimize the deviations from Gaussianity caused by the orbital motion. We employ the uncertainty data offered in equinoctial elements. The covariance matrix we use for the sampling accounts for the uncertainty in the six equinoctial elements.

We propagate each sample using the STM of the nominal orbit of the object of study (Eq. (27)). If the nominal orbit intrudes the sphere of a given radius centered at the Earth, the heliocentric propagation is interrupted and all the MC samples ($i = 1, \ldots, M$) are transformed from the heliocentric to the geocentric reference frame. In the geocentric phase, we consider a reference frame with origin in the Earth center and having the same orientation of the heliocentric inertial frame. We compute the relative positions and velocities with respect to the Earth by

$$\hat{\boldsymbol{r}}_i = \boldsymbol{r}_i - \boldsymbol{r}_\oplus \tag{43}$$

$$\hat{\boldsymbol{v}}_i = \boldsymbol{v}_i - \boldsymbol{v}_\oplus \tag{44}$$

where we denote the geocentric variables with a hat ($\hat{}$), and employ $\oplus$ as the Earth symbol.

From $\hat{\boldsymbol{r}}_i$, $\hat{\boldsymbol{v}}_i$ we obtain the geocentric Dromo representation of the MC samples, which are propagated again using linear theory until the distance between the nominal orbit and the Earth is greater than the employed threshold. At that point, another primary body switch back to the heliocentric frame is performed using Eqs. (43, 44). The switch is repeated if needed in case the nominal orbit comes again close to the Earth. A scheme of this process is shown in Fig. 3.

The switch is calculated using Eqs. (22, 23, 43, 44) and the expressions in Appendix A that provide the Dromo elements as a function of the inertial Cartesian state vector. This set of equations is constituted by fully analytical expressions involving the position and velocities of the asteroid and the Earth, and in general is nonlinear. When performing a switch, a Gaussian distribution will remain Gaussian if the eigenvalues of its covariance matrix are sufficiently small, because in that case the equations that define the switch can then be linearized around the reference orbit with negligible error. A second switch under

similar conditions will yield a final distribution that will also be approximately Gaussian. Moreover, for primary body switches that are well approximated by a linear mapping, a combination of switches with heliocentric and geocentric STMs will result in a STM which is mathematically equivalent to the purely heliocentric STM. On the other hand, if the equations that govern the primary body switch cannot be replaced by their linearized form, Gaussianity will not be conserved in general. We note that close orbits can still be propagated using a STM even if they follow a non-Gaussian distribution. That is, we can combine linear propagation arcs with primary body switches, retaining with a higher degree of fidelity the nonlinearities of the orbital motion. The uncertainty distribution at a generic epoch is characterized by the dispersed MC states, and if necessary, the covariance matrix and other higher order moments can be estimated [28, pp. 341-363].

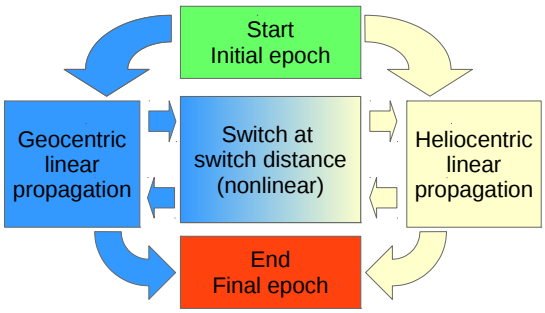

Figure 3: Primary body switch flow chart.

We highlight that the primary body switch, when applied to the orbit uncertainty propagation problem, is a technique that seeks reducing the third-body gravitational perturbation *linearization error* of the orbital uncertainty dispersion. This is different from the classical application of the primary body switch, which aims to reduce the *numerical error* of a single orbit [25].

5. Results

In this section we present examples of orbit uncertainty propagation for some selected asteroids employing the primary body switch strategy.

These asteroids were chosen as good candidates to perform the primary body switch based on two criteria. First, all of them have their closest approach before the year 2050 at a distance no much greater than 1 radius of the Sphere of Influence of the Earth $R_{\mathrm{SoI}} \simeq 0.0062\,\mathrm{au} \simeq 9.25 \times 10^5\,\mathrm{km}$. For reference, 1 lunar distance corresponds to $384400\,\mathrm{km} \simeq 0.42\,R_{\mathrm{SoI}}$. Second, they have a well determined orbit. Here, we employ the Orbit Condition Code (OCC) to decide whether to apply the switch or not to a particular asteroid. The OCC provides an estimate of how well determined is an orbit and takes integer values from 0 to 9, where 0 is assigned to extremely well determined orbits and 9 represents very large uncertainties. It is mathematically defined as

$$OCC = \left\lfloor \ln \frac{\dot{\lambda}}{\dot{\lambda}_0} + 1 \right\rfloor, \tag{45}$$

where $\lfloor y \rfloor$ is the floor function, $\dot{\lambda}_0 \simeq 1.49$ and the longitude runoff $\dot{\lambda}$ is

$$\dot{\lambda} = \left(e\,\sigma_{T_p}\big|_{\mathrm{d}} + 10\,\sigma_P\big|_{\mathrm{d}}\,\frac{1}{P\big|_{\mathrm{y}}} \right) k \frac{1}{P\big|_{\mathrm{y}}} \times 3600 \times 3. \tag{46}$$

In this equation, $\sigma_{T_p}\big|_{\mathrm{d}}$ is the standard deviation of the perihelion passage time in days, $P\big|_{\mathrm{y}}$ is the orbital period in years, $\sigma_P\big|_{\mathrm{d}}$ is the standard deviation of the orbital period in days and $k = \frac{180}{\pi} 0.01720209895$ deg is the Gaussian constant in degrees. We note that the floor function can be dropped from Eq. (45), if needed, to better quantify the uncertainty of an orbit [21]. We only selected asteroids with initial OCC equal to 0 or 1.

The selected asteroids are shown in Table 1. For all these asteroids, we performed a parametric search on the switch distance to analyze its effect on the propagation accuracy. We took as lower bound the minimum close approach distance, and consider performing a switch as far as 3 radii of the Sphere of Influence of the Earth.

Table 1: Significant data of the asteroids considered in the analysis.

Asteroid	OCC	Closest approach distance [R_{SoI}]	Closest approach epoch	Final propagation epoch
2011AG5	1	1.17	2040-02-04	2050-01-01
2012AP10	1	0.51	2042-12-29	2050-01-01
2004RQ252	1	0.57	2043-04-01	2050-01-01
2001AV43	0	0.34	2029-11-11	2040-01-01
99942 Apophis	0	0.04	2029-04-13	2040-01-01

To better understand the effect of the primary body switch, we also considered cases where the initial standard deviations, expressed in equinoctial elements, were scaled up or down by a factor of 10.

We used as a measure of the linearization error the position error averaged over all the MC samples:

$$\epsilon = \frac{1}{M} \sum_{i=1}^{M} \sqrt{(x_i - x_i^*)^2 + (y_i - y_i^*)^2 + (z_i - z_i^*)^2} \tag{47}$$

where the true solution $(x_i^*, y_i^*, z_i^*)^\top$ was calculated by integrating the equations of motion for each individual sample. Furthermore, for each asteroid and initial uncertainty scaling factor, we normalized the average error with the maximum position standard deviation estimated from the true solution at the final epoch.

5.1. 2011AG5

The orbit uncertainty propagation of 2011AG5, a Potential Hazardous Asteroid (PHA), was carried out using the primary body switch. 2011AG5 will experience a close approach with the Earth in 2040 February 4 with a minimum distance of about 0.007 au, which is slightly larger than the radius of the Sphere of Influence. The propagation was performed from 2011 November 29, and the average error was evaluated on 2050 January 1.

Figure 4 shows the average error as a function of the switch distance for this asteroid at the end of the propagation. If the switch distance is smaller than

the closest approach distance, the switch cannot be performed. However, for distances of about 1.05 times the Earth closest approach distance, the average error drops between one and two orders of magnitude. This behavior persists even when scaling up or down the initial uncertainty, which suggests that for 2011AG5, performing a switch may help to greatly reduce the uncertainty propagation error. The gray region in Fig. 4 corresponds to a switch distance between 1.05 and 1.15 times the closest approach distance of the nominal orbit.

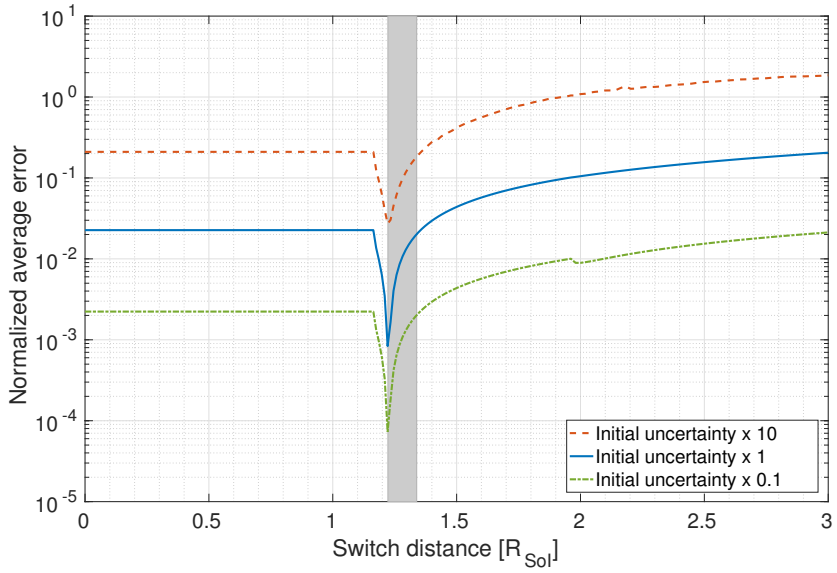

Figure 4: Average position error for 2011AG5 at year 2050 as a function of the switch distance. For the real initial covariance, the normalization factor is about 1.8×10^6 km. The gray region corresponds to a switch distance between 1.05 and 1.15 times the closest approach distance of the nominal orbit.

5.2. 2012AP10

2012AP10 is a 20 m asteroid that will flyby the Earth in 2042 December 29 at a nominal distance of about 1.4 lunar distances, but its minimum distance with the Earth could be as low as 0.4 lunar distances. This is reflected in its condition code of 1. We propagate from 2013 April 5 to 2050 January 1, and evaluate the average error at the end of the propagation. As it can be seen in

Fig. 5, the average error is effectively reduced for the actual initial uncertainty, as well as for its scaled-up initial covariance matrix. However, by lowering the initial uncertainty the switch becomes less effective in this case.

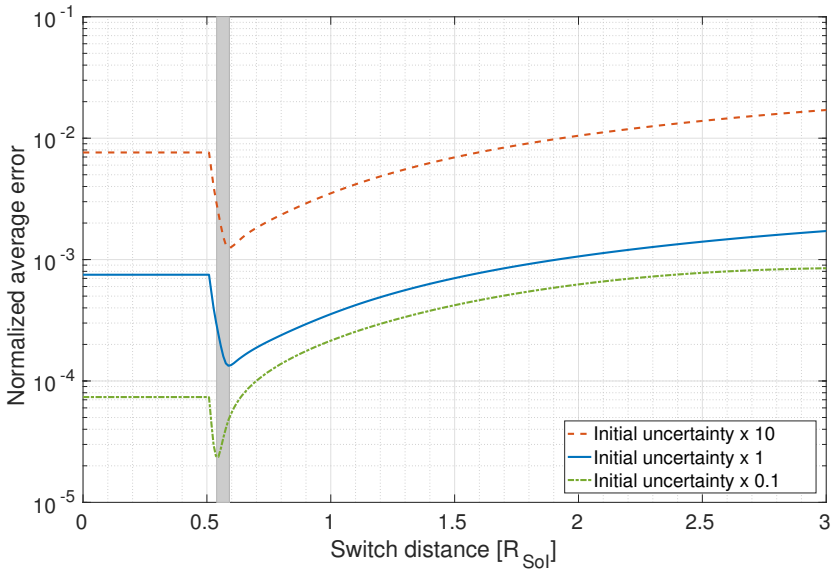

Figure 5: Average position error for 2012AP10 at year 2050 as a function of the switch distance. For the real initial covariance, the normalization factor is about 1.3×10^5 km. The gray region corresponds to a switch distance between 1.05 and 1.15 times the closest approach distance of the nominal orbit.

5.3. 2004RQ252

2004RQ252 will flyby the Earth at a distance of about 8×10^5 km in 2043 April 1. Our integration starts in 2006 March 5, and is performed until 2050 January 1. Figure 6 shows the average position error at the final epoch. The effectiveness of the switch with this asteroid resembles that of 2011AG5, with a very high efficiency for a switch performed at a distance of about 1.05 times the Earth closest approach distance.

For 2004RQ252, we also provide a comparison between the Dromo linear propagation without performing any switch, and a linear propagation in Cartesian coordinates. Figure 7 shows how the Dromo linear method outperforms

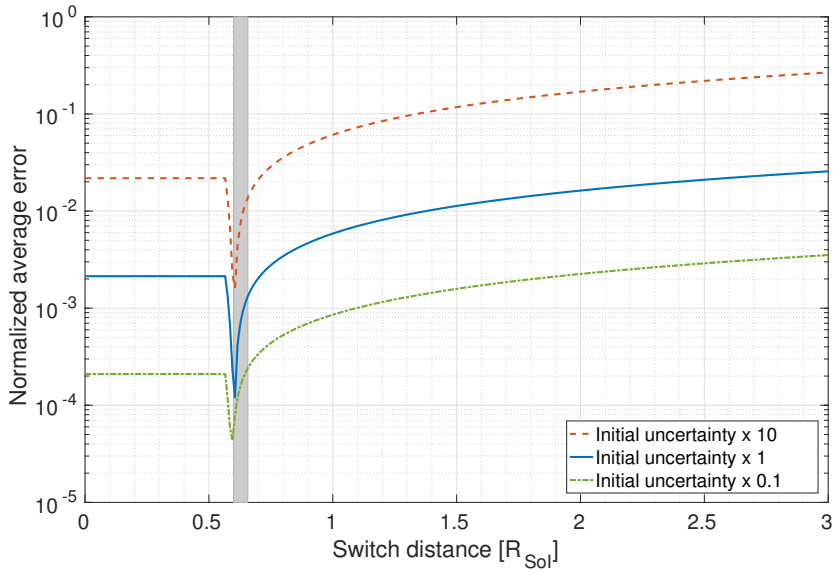

Figure 6: Average position error for 2004RQ252 at year 2050 as a function of the switch distance. For the real initial covariance, the normalization factor is about 1.6×10^5 km. The gray region corresponds to a switch distance between 1.05 and 1.15 times the closest approach distance of the nominal orbit.

its Cartesian counterpart until the 2043 flyby. After this close encounter, the error of the two methods is comparable. By employing the primary body switch strategy, the final error can be reduced by a factor of 17.75.

5.4. 2001AV43

The propagation of the orbit uncertainty of 2001AV43 was performed starting from 2012 October 14, and was carried out until 2040 January 1. In this interval, 2001AV43 has an Earth flyby on 2029 November 11, approaching as close as $0.34\,R_{\mathrm{SoI}}$.

Figure 8 shows the results of the primary body switch evaluated at the final epoch. For the actual or the scaled-down initial orbit uncertainty, the advantages of performing a primary body switch are not clear. This could be explained by its well-determined orbit, which has an OCC of 0. When considering larger initial uncertainty, a switch at distances of about three times

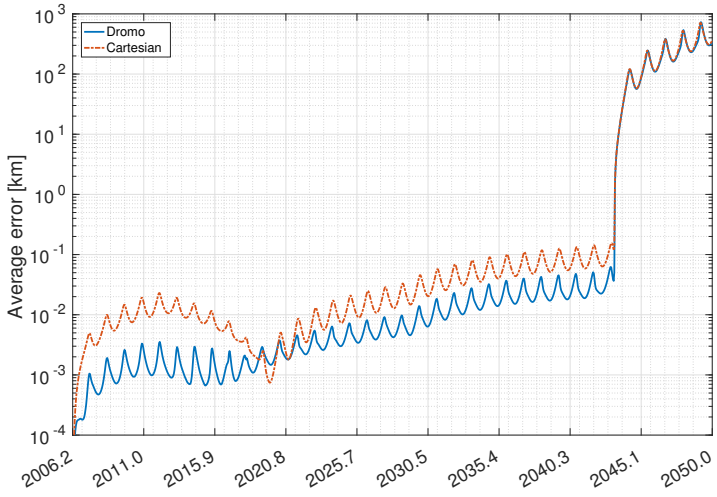

Figure 7: Average position error for 2004RQ252As a function of time.

the closest approach distance reduces the final error in more than half. We note that for 2001AV43, the closest approach occurs at a distance of the same order of magnitude as the Moon distance, whose gravity at close distances may affect the accuracy of the linear propagation.

5.5. 99942 Apophis

We applied the proposed primary body switch to the PHA Apophis. The propagation starts on 2009 May 6 and is performed until 2040 January 1, when we evaluate the average position error. In 2029, Apophis will fly by the Earth at a nominal closest-approach distance of about 38000 km. During this close flyby, the nonlinear nature of the Earth's gravitational force across the uncertainty region may strongly affect the evolution of the orbit uncertainty of this asteroid.

Figure 9 shows the results of performing the primary body switch at different distances from the Earth and for different scalings of the initial uncertainty. For the actual initial uncertainty, the error can be reduced by 40% if a switch is performed at about $0.6\,R_{\mathrm{SoI}}$. Similar results are obtained when considering larger initial uncertainties, where the reduction increases to almost 70%. However, a

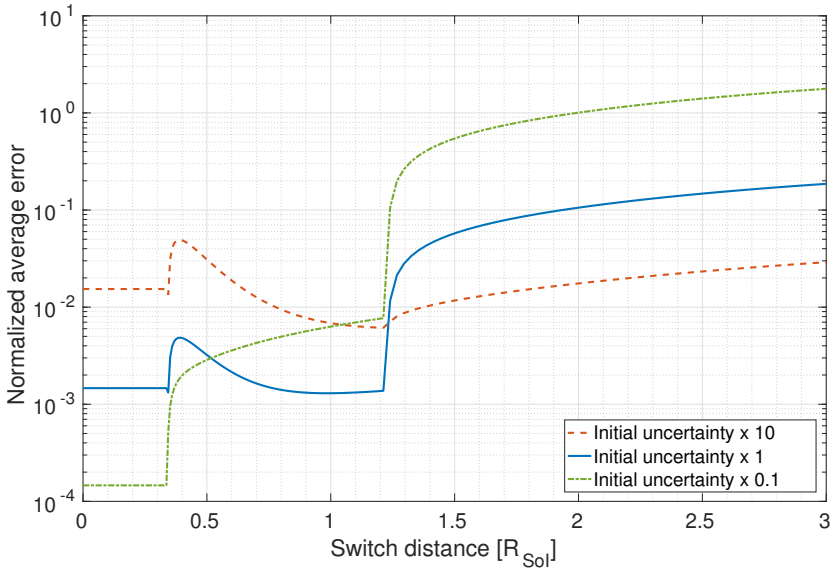

Figure 8: Average position error for 2001AV43 at year 2040 as a function of the switch distance. For the real initial covariance, the normalization factor is about 2.9×10^5 km.

scaled-down initial uncertainty does not seem to benefit from the primary body switch.

6. Discussion

Figure 10 shows the optimum distance that minimizes the final average error. Figure 11 shows the switch error-reduction factor, which is defined as the ratio of the error that we have without performing the switch to the minimum error that we obtain among all the possible switch distances. That is, a higher value of the error-reduction factor means that the switch is a more effective way of decreasing the error for that particular case. The results are summarized in Table 2. In Table 3, we provide the closest approach distance with respect to the Earth and the Moon for each asteroid. For 2001AV43 and Apophis, the switch did not reduce the error for a scaling factor of 1. We indicated this in Table 2 as N/A (not applicable).

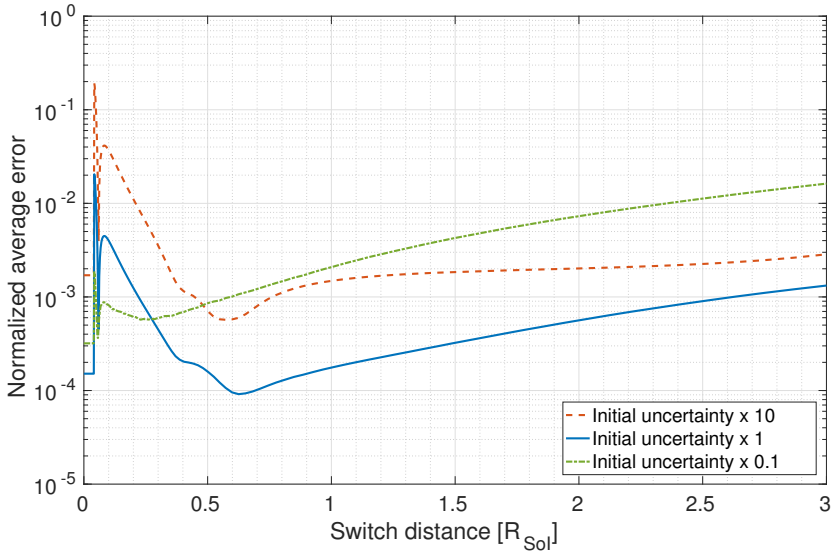

Figure 9: Average position error for 99942 Apophis at year 2040 as a function of the switch distance. For the real initial covariance, the normalization factor is about 2.9×10^5 km.

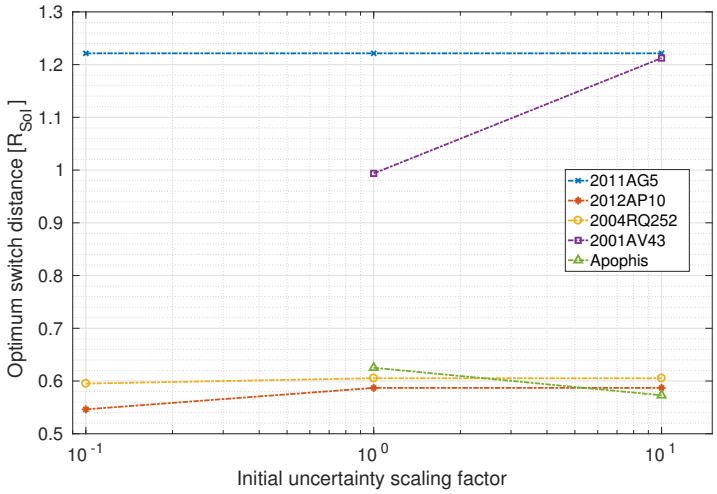

Figure 10: Optimum switch distance. For 2001AV43 and Apophis, the switch did not reduce the error for a scaling factor of 1.

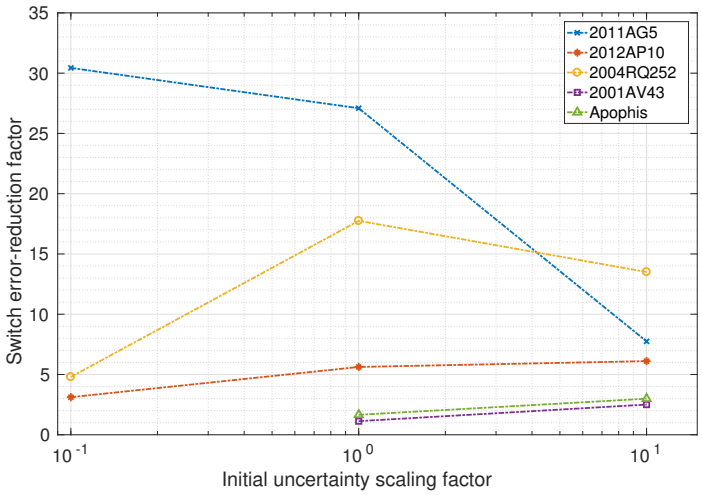

Figure 11: Switch error-reduction factor. For 2001AV43 and Apophis, the switch did not reduce the error for a scaling factor of 1.

2011AG5, 2012AP10 and 2004RQ252 are characterized by having an optimum switch distance that does not vary significantly with the initial uncertainty scaling factor, and corresponds to a switch distance slightly larger than the closest approach distance. The optimum switch distance lays between a 5% and a 15% larger than the minimum close approach distance with respect to the Earth. For these asteroids, performing the switch over very short propagation arcs improves drastically the result of the uncertainty propagation. This is justified because near the close approach is where the linearization error of Earth's gravity becomes critical [21]. However, longer geocentric propagation arcs are not beneficial in these cases because the Sun gravity linearization error would become dominant.

On the other hand, a less clear behavior is observed for Apophis and 2001AV43. In the case of Apophis, the nonlinearity of its very close flyby causes multiple local minima in the curve of average error for some of the initial uncertainty scaling factors. Additionally, during the 2029 close encounter, Apophis comes as close to the Moon as 6.5×10^{-4} au, which further complicates the propaga-

Table 2: Summary of the results. For 2001AV43 and Apophis, the switch did not reduce the error for a scaling factor of 1.

Asteroid	Scaling factor	Optimum switch distance [R_{SoI}]	Error-reduction factor	$\frac{\text{Optimum switch distance}}{\text{Minimum Earth distance}}$
2011AG5	0.1	1.22	30.44	1.05
	1	1.22	27.09	1.05
	10	1.22	7.75	1.05
2012AP10	0.1	0.55	3.12	1.06
	1	0.59	5.63	1.14
	10	0.59	6.11	1.14
2004RQ252	0.1	0.60	4.80	1.04
	1	0.61	17.75	1.06
	10	0.61	13.51	1.06
2001AV43	0.1	0.34	N/A	N/A
	1	0.99	1.13	2.92
	10	1.21	2.51	3.57
99942 Apophis	0.1	0.04	N/A	N/A
	1	0.63	1.66	15.04
	10	0.57	2.99	14.11

tion of the uncertainty. For 2001AV43, the results suggest that the initial orbit uncertainty could be too small to benefit from the switch, or that the linearization error of the Moon gravity during the flyby has a non-negligible importance. The closest approach distance of these two asteroids with the Earth is below 2.5×10^{-3} au (about the Earth-Moon distance), which could suggest that this is a limiting factor on the applicability of the primary body switch technique with the current formulation. To assess the frequency of such close Earth encounters, we searched the NEODyS database for the number of encounters with different maximum closest-approach distance. We carried out our query for encounters occurring at any epoch, and repeated the process for encounters only after the

Table 3: Summary of closest approaches.

Asteroid	Earth-asteroid minimum distance [au]	Moon-asteroid minimum distance [au]
2011AG5	7.2×10^{-3}	4.7×10^{-3}
2012AP10	3.2×10^{-3}	5.4×10^{-3}
2004RQ252	3.5×10^{-3}	1.3×10^{-3}
2001AV43	2.1×10^{-3}	1.7×10^{-3}
99942 Apophis	2.5×10^{-4}	6.5×10^{-4}

current epoch. Our search reveals 1785 close encounters in the future with a minimum nominal distance from the Earth smaller than $3\,R_{\mathrm{SoI}} \simeq 0.0185\,\mathrm{au}$. Among them, only 60 encounters occur closer than the Moon distance $a_{\leftmoon} = 0.00257\,\mathrm{au}$. The full result of our search is shown in Table 4.

Table 4: Statistics of Earth encounters after a search in the NEODyS database.

Maximum close-approach distance	Close encounters (in the future)	Close encounters (any epoch)
$3\,R_{\mathrm{SoI}} = 0.0185\,\mathrm{au}$	1784	5369
$2a_{\leftmoon} = 0.00514\,\mathrm{au}$	196	1046
$a_{\leftmoon} = 0.00257\,\mathrm{au}$	60	455

Finally, from the summary in Tables 2 and 3, a larger Earth-asteroid minimum distance seems to be correlated with a higher error-reduction factor. However, a more detailed study and a wider population of Earth-encountering asteroids are needed to understand this relation.

7. Conclusion

In this work, we extended the domain of validity of linear propagation in Dromo elements in the presence of planetary close encounters. We combined linear propagation in the heliocentric and geocentric frames with nonlinear transformations of the Dromo elements between the two. By using this approach,

the linearization error of the third body gravitational force can be reduced when linearly propagating the orbit uncertainty.

We applied the method to a list of asteroids that have a close approach with the Earth before 2050, and with an Orbit Condition Code not greater than 1. We also scaled up and down by a factor of ten the standard deviations at the initial epoch to study how larger or smaller uncertainties affect the applicability of the method. We found that performing the primary body switch may improve the result of the linear propagation up to a factor of 30, and that in many cases a switch on very short arcs may drastically improve the orbit uncertainty prediction.

In future works, we will consider a broader set of asteroids, both real and simulated, to better understand the role of the switch distance. An alternative formulation for the geocentric arc, which could improve the accuracy of the method, is also under study.

Acknowledgments

The Ministry of Education, Culture, Sports, Science and Technology (MEXT) of the Japanese government supported Javier Hernando-Ayuso under its program of scholarships for graduate school students.

The work of Claudio Bombardelli was supported by the Spanish Ministry of Economy and Competitiveness within the framework of the research project "Dynamical Analysis, Advanced Orbital Propagation, and Simulation of Complex Space Systems" (ESP2013-41634-P).

Finally, the authors would like to thank the anonymous reviewer and Giovanni Valsecchi for their helpful comments and suggestions.

References

[1] P. S. Maybeck, Stochastic models, estimation, and control Volume 2, volume 141-2 of *Mathematics in Science and Engineering*, Academic press, New York, 1982.

[2] R. S. Park, D. J. Scheeres, Nonlinear mapping of Gaussian statistics: theory and applications to spacecraft trajectory design, Journal of guidance, Control, and Dynamics 29 (2006) 1367–1375.

[3] R. Armellin, P. Di Lizia, F. Bernelli-Zazzera, M. Berz, Asteroid close encounters characterization using differential algebra: the case of Apophis, Celestial Mechanics and Dynamical Astronomy 107 (2010) 451–470.

[4] D. Giza, P. Singla, M. Jah, An approach for nonlinear uncertainty propagation: Application to orbital mechanics, in: AIAA Guidance, Navigation, and Control Conference, 2009-6082, Chicago, Illinois, 2009. doi:10.2514/6.2009-6082.

[5] S. J. Julier, J. K. Uhlmann, A new extension of the kalman filter to nonlinear systems, in: The 11th International Symposium on Aerospace/Defence, Sensing, Simulation and Controls, volume 3, Orlando, FL, 1997, pp. 182–193.

[6] B. A. Jones, A. Doostan, G. H. Born, Nonlinear propagation of orbit uncertainty using non-intrusive polynomial chaos, Journal of Guidance, Control, and Dynamics 36 (2013) 430–444.

[7] V. Vittaldev, R. P. Russell, R. Linares, Spacecraft uncertainty propagation using gaussian mixture models and polynomial chaos expansions, Journal of Guidance, Control, and Dynamics 39 (2016) 2615–2626.

[8] C. Tardioli, M. Kubicek, M. Vasile, E. Minisci, A. Riccardi, Comparison of non-intrusive approaches to uncertainty propagation in orbital mechanics, AAS 15-545, American Astronautical Society, San Diego, California, 2015, pp. 3979–3992.

[9] A. Milani, M. E. Sansaturio, G. Tommei, O. Arratia, S. R. Chesley, Multiple solutions for asteroid orbits: computational procedure and applications, Astronomy & Astrophysics 431 (2005) 729–746.

[10] J. L. Junkins, M. R. Akella, K. T. Alfriend, Non-Gaussian error propagation in orbital mechanics, The Journal of the Astronautical Sciences 44 (1996) 541–563.

[11] J. Hernando-Ayuso, C. Bombardelli, Orbit covariance propagation via quadratic-order state transition matrix in curvilinear coordinates, Celestial Mechanics and Dynamical Astronomy 129 (2017) 215–234.

[12] V. T. Coppola, S. Tanygin, Using bent ellipsoids to represent large position covariance in orbit propagation, Journal of Guidance, Control, and Dynamics 38 (2015) 1775–1784.

[13] R. G. Melton, Time-explicit representation of relative motion between elliptical orbits, Journal of Guidance, Control, and Dynamics 23 (2000) 604–610.

[14] C. M. Lane, P. Axelrad, Formation design in eccentric orbits using linearized equations of relative motion, Journal of Guidance, Control, and Dynamics 29 (2006) 146–160.

[15] K. Hill, K. Alfriend, C. Sabol, Covariance-based uncorrelated track association, in: AIAA/AAS Astrodynamics Specialist Conference, AIAA 2008-7211, Honolulu, Hawaii, 2008.

[16] J. Peláez, J. M. Hedo, P. R. de Andrés, A special perturbation method in orbital dynamics, Celestial Mechanics and Dynamical Astronomy 97 (2007) 131–150.

[17] H. Urrutxua, M. Sanjurjo-Rivo, J. Peláez, Dromo propagator revisited, Celestial Mechanics and Dynamical Astronomy 124 (2015) 1–31.

[18] G. Baù, C. Bombardelli, J. Peláez, A new set of integrals of motion to propagate the perturbed two-body problem, Celestial Mechanics and Dynamical Astronomy 116 (2013) 53–78.

[19] G. Baù, C. Bombardelli, Time elements for enhanced performance of the dromo orbit propagator, The Astronomical Journal 148 (2014) 43.

[20] G. Baù, C. Bombardelli, J. Pelez, E. Lorenzini, Non-singular orbital elements for special perturbations in the two-body problem, Monthly Notices of the Royal Astronomical Society 454 (2015) 2890–2908.

[21] J. Hernando-Ayuso, C. Bombardelli, Orbit Uncertainty Propagation Using Dromo, in: AIAA/AAS Astrodynamics Specialist Conference, AIAA 2016-5632, 2016. doi:10.2514/6.2016-5632.

[22] J. Hernando-Ayuso, C. Bombardelli, Orbit uncertainty propagation around non-spherical bodies using the Dromo formulation, in: 26th International symposium on Space Flight Dynamics, held together the 31st International Symposium on Space Technology and Science, 2017-d-071, Matsuyama, Japan, 2017.

[23] J. Roa Vicens, J. Peláez Álvarez, Efficient trajectory propagation for orbit determination problems, in: AAS/AIAA Astrodynamics Specialist Conference, AAS-15-730, Univelt, Vail, Colorado, USA, 2015.

[24] J. Roa, J. Peláez, The theory of asynchronous relative motion i: time transformations and nonlinear corrections, Celestial Mechanics and Dynamical Astronomy 127 (2017) 301–330.

[25] D. Amato, G. Baù, C. Bombardelli, Accurate orbit propagation in the presence of planetary close encounters, Monthly Notices of the Royal Astronomical Society 470 (2017) 2079–2099.

[26] W. M. Folkner, J. G. Williams, D. H. Boggs, R. S. Park, P. Kuchynka, The planetary and lunar ephemerides DE430 and DE431, Interplanetary Network Progress Report 42-196 196 (2014) 1–81.

[27] Simon, J.-L., Francou, G., Fienga, A., Manche, H., New analytical planetary theories VSOP2013 and TOP2013, Astronomy & Astrophysics 557 (2013) A49.

[28] H. Cramér, Mathematical Methods of Statistics, Princeton University Press, Princeton, 1946.

Appendix A. Cartesian coordinates to Dromo elements transformation

The inverse of the transformation given by Eqs. (22–23) constitutes an alternative of Eqs. (16–21) for setting the initial values of the Dromo variables [18]

$$q_1 = \left(\frac{h^2}{r} - 1\right)\cos\sigma_0 + h\,u\sin\sigma_0, \tag{A.1}$$

$$q_2 = \left(\frac{h^2}{r} - 1\right)\sin\sigma_0 - h\,u\cos\sigma_0, \tag{A.2}$$

$$q_3 = 1/h, \tag{A.3}$$

$$q_4 = \frac{1}{4q_7}\left\{\left(\frac{h_x y - h_y x}{rh}\right)\cos\sigma_0 + \frac{z}{r}\sin\sigma_0 - \frac{h_y}{h}\right\}, \tag{A.4}$$

$$q_5 = \frac{1}{4q_7}\left\{\left(\frac{h_x y - h_y x}{rh}\right)\sin\sigma_0 - \frac{z}{r}\cos\sigma_0 + \frac{h_x}{h}\right\}, \tag{A.5}$$

$$q_6 = \frac{1}{4q_7}\left\{\left(-\frac{x}{r} - \frac{h_z x - h_x z}{rh}\right)\sin\sigma_0 + \left(\frac{y}{r} - \frac{h_y z - h_z y}{rh}\right)\cos\sigma_0\right\}, \tag{A.6}$$

$$q_7 = \pm\frac{1}{2}\sqrt{1 + \frac{h_z}{h} + \left(\frac{x}{r} + \frac{h_z x - h_x z}{rh}\right)\cos\sigma_0 + \left(\frac{y}{r} - \frac{h_y z - h_z y}{rh}\right)\sin\sigma_0}, \tag{A.7}$$

$$\sigma = \sigma_0 = \nu_0 + \beta = \operatorname{atan2}\left(h\,u, \frac{h^2}{r} - 1\right) + \beta, \tag{A.8}$$

where $\boldsymbol{h} = (h_x, h_y, h_z)^\top = \boldsymbol{r} \times \boldsymbol{v}$, and the radial velocity u reads

$$u = \frac{\boldsymbol{r}\cdot\boldsymbol{v}}{r}. \tag{A.9}$$

If $q_7 = 0$, the following expressions may be used:

$$q_4 = \frac{1}{2q_6}\frac{h_x}{h}, \tag{A.10}$$

$$q_5 = \frac{1}{2q_6}\frac{h_y}{h}, \tag{A.11}$$

$$q_6 = \pm\sqrt{\frac{1}{2}\left(1 + \frac{h_z}{h}\right)}. \tag{A.12}$$

For the case of q_6 and q_7 being both zero, the inclination corresponds to 180 deg and the quaternion is defined by

$$q_4 = \pm \sqrt{\frac{1}{2}\left(1 - \left(\frac{y}{r}\sin\sigma_0 + \frac{h_z x - h_x z}{hr}\cos\sigma_0\right)\right)}, \tag{A.13}$$

$$q_5 = \frac{1}{2q_4}\left(\frac{x}{r}\sin\sigma_0 + \frac{h_y z - h_z y}{hr}\cos\sigma_0\right). \tag{A.14}$$

Finally if $q_4 = q_6 = q_7 = 0$, then $q_5 = \pm 1$.